UCLA-ENG-7249
July 1972

ACOUSTIC EMISSION AND FRACTURE MECHANICS TESTING OF METALS AND COMPOSITES

A. S. Tetelman
Materials Department

School of Engineering and Applied Science
University of California
Los Angeles, California

Unclassified

Security Classification

DOCUMENT CONTROL DATA - R & D

(Security classification of title, body of abstract and indexing annotation must be entered when the overall report is classified)

1. ORIGINATING ACTIVITY (Corporate author)
University of California, Los Angeles

2a. REPORT SECURITY CLASSIFICATION
Unclassified

2b. GROUP
NA

3. REPORT TITLE
Acoustic Emission and Fracture Mechanics Testing of Metals and Composites

4. DESCRIPTIVE NOTES (Type of report and inclusive dates)
Technical Report

5. AUTHOR(S) (First name, middle initial, last name)
A. S. Tetelman

6. REPORT DATE
July 1972

7a. TOTAL NO. OF PAGES
45

7b. NO. OF REFS

8a. CONTRACT OR GRANT NO.
DAHC04 69 C 0008

b. PROJECT NO.
20061102B32D

c.

d.

9a. ORIGINATOR'S REPORT NUMBER(S)
NA

9b. OTHER REPORT NO(S) (Any other numbers that may be assigned this report)
8016.6-MC

10. DISTRIBUTION STATEMENT
Approved for public release; distribution unlimited.

11. SUPPLEMENTARY NOTES
None

12. SPONSORING MILITARY ACTIVITY
U. S. Army Research Office-Durham

13. ABSTRACT

Acoustic Emission testing has found many uses in recent years and new applications are constantly being uncovered. One of the most fruitful areas for application lies in the characterization of microscopic processes of yielding and fracture, and macroscopic processes of slow crack growth and onset of fast crack propagation. This paper has described these processes and emphasized that the total counts and count rate depend on the energy released per event and the density of events per unit of deformation. The models presented herein are first order approximations which await confirmation.

14. KEY WORDS
Acoustic Emission Testing
Crack Propagation
Fracture Mechanics
Metals
Composites

DD FORM 1 NOV 68 1473 REPLACES DD FORM 1473, 1 JUN 64, WHICH IS OBSOLETE FOR ARMY USE.

Unclassified

Security Classification

UCLA-ENG 7249
July 1972

ACOUSTIC EMISSION AND FRACTURE MECHANICS

TESTING OF METALS AND COMPOSITES

A.S. Tetelman

Materials Department
School of Engineering and Applied Science
University of California
Los Angeles, California

Presented at
U.S. – Japan Joint Symposium on Acoustic Emission
Tokyo, Japan
Technical Report No. 7

July 1972

DAH-04-68-C-0008

Prepared for the U.S. Army Research Office – Durham

I. Introduction

During the last several years the field of acoustic emission testing has grown very rapidly.[1,2] This growth has been stimulated by 1) the realization that acoustic emission can be used to characterize and monitor the processes of flow and fracture that occur in metals and composites during mechanical testing and 2) the availability of commercial testing equipment at modest cost. Acoustic emission testing has been utilized in several ways:[2]

a) as a research tool to help understand various processes of flow and fracture;

b) as a monitor of slow crack growth in structural components;

c) as a monitor of specific phenomena, such as weld cracking or susceptibility to stress corrosion cracking;

d) as part of a large scale, computerized system designed to monitor large structures against premature failure, particularly during proof testing.

The growth of acoustic emission testing has paralleled our increased understanding of plastic flow and crack propagation in structural materials. Acoustic emission testing (AET) is the only method of non-destructive inspection whose signal output can be directly correlated with the crack tip stress intensity factor K, the sole parameter that describes both the rate of slow crack growth in fatigue and/or reactive environments and the conditions for the onset of unstable crack propagation. This correlation provides the principal driving force for the development of acoustic emission testing in the last few years, and its application to failure prevention in large structural systems.

This report reviews some of the principal correlations between AET and the processes of flow and fracture in structural materials. We begin with

a short review of the principal aspects of fracture mechanics and show how various parameters can be used to predict the conditions for structural failure. We then discuss the nature of the information that can be gained from AET, and show how this correlates with fracture mechanics parameters. Finally, we discuss some specific applications where AET offers great promise as a failure prevention tool.

II. Principles of Fracture Mechanics

Most structural materials contain flaws or cracks that are introduced during fabrication (e.g., weld defect) or during service (e.g., a corrosion pit). Under various combinations of static and alternating loads and reactive environments, these flaws grow slowly and stably. Unstable fracture occurs in a structure when a flaw has developed to a critical size that is a function of both the applied (or residual) stresses acting on the structure and the toughness of the material. The principles of linear elastic fracture mechanics can be used to describe these functional relationships for unstable fracture that occur at stresses below the general yield stress.

For simplicity, we consider a plate of thickness B and width W that contains a sharp, through crack of length 2a and tip radius ρ. (Fig. 1) When the plate is subjected to a uniform gross section stress σ, two effects take place. First, the crack tip faces are opened by an amount that is called the crack tip opening displacement (COD). Second, the material within a zone of radius R from the tip is plastically strained to accommodate this crack tip displacement. The (COD) and R are related through the equation[3]

$$(\text{COD}) = \beta \frac{\sigma_Y}{E} R \qquad (1)$$

where σ_Y is the tensile yield strength, E is the elastic modulus, and β is a numerical constant that varies between 2 and 4 depending on the mode of

loading of the crack faces and the degree of plastic constraint at the crack tip. Inside the plastic zone, the plastic strains ε_L vary inversely with distance r from the crack tip. Likewise, in sharply cracked materials, the combination of plastic constraint and strain hardening cause the peak tensile stresses σ_L to reach a value of approximately $3\sigma_y$ close to the tip, and then to diminish with distance from the crack tip. Crack extension occurs when a critical strain[3] or critical stress[4,5] is achieved at the crack tip:

$$\sigma_L = \sigma_f^* \quad \text{(cleavage)} \tag{2a}$$

$$\varepsilon_L = \varepsilon_f^* \quad \text{(rupture)} \tag{2b}$$

Since both the local stress and the local strain are functions of the (COD), the generalized condition for unstable fracture can be written as

$$(\text{COD}) = (\text{COD})_c \tag{3}$$

In a non or weakly strain hardening material the stresses in the plastic zone near the crack tip are of the order of the constrained yield strength $3\sigma_y$. Consequently, the work done G at the crack tip is (approximately) equal to the product of the local stress acting on the volume element adjacent to the tip, and the displacement over which it acts:[3]

$$G \cong 3\sigma_Y \frac{\pi}{4} (\text{COD}) \tag{4}$$

a critical (COD) for fracture therefore implies that a critical work is required for fracture, i.e.,

$$G = G_c \ . \tag{5}$$

The work done at the crack tip, as well as the (COD) and plastic zone size R, is a function of the key parameter in linear elastic fracture mechanics technology, the stress intensity factor K. When the plastic zone at the crack tip is small and is surrounded by elastic material, it is possible to

describe the crack by the local stresses that would have existed at and near its tip <u>if</u> the material had not yielded locally.

A parameter K is defined[6]

$$\lim_{\rho \to 0} K = \frac{\sigma_{MAX}}{2} \sqrt{\pi\rho} \tag{6}$$

which is a function of the maximum stress at the tip of this crack (σ_{max}) in the limit as the root radius $\rho \to 0$, assuming the material had remained perfectly elastic (which of course, it does not). For example, for an elliptical center crack of length 2a that extends all the way through the thickness

$$\sigma_{MAX} = \sigma K_t = \sigma(1 + 2\sqrt{a/\rho} \tag{7}$$

so

$$K = \sigma \sqrt{\pi a} \tag{8}$$

Thus, K is a direct function of the applied stress σ and the elastic stress concentration factor K_t. For other crack shapes and loading modes, K_t will vary. However, in all cases

$$K = \sigma \sqrt{\pi a}\ f(g) \tag{9}$$

where f(g) is a geometrical parameter of the order of unity that can be determined analytically. These equations only apply when $\sigma < \sigma_y$, such that general yield has not occurred across the net section ahead of the crack. Under plane strain tensile loading, the plastic zone size R increases with the (K/σ_y) ratio:

$$R \cong \frac{1}{3\pi} \left(\frac{K}{\sigma_y} \right)^2 \tag{10}$$

From Equation (1) with $\beta = 4$ we then have

$$(COD) = \frac{4}{3\pi E} \sigma_Y \left(\frac{K}{\sigma_Y} \right)^2 \qquad (\sigma < \sigma_Y) \qquad (11)$$

and hence from Equation (4) we find

$$G = \frac{K^2}{E} \qquad (\sigma < \sigma_Y) \qquad (12)$$

The microscopic fracture criteria (Equations (2a) and (2b)) which lead to macro fracture criteria at the crack tip (Equations (3) and (5)), in turn indicate that unstable fracture occurs when K achieves a critical value

$$K = K_c \qquad (13)$$

where

$$K_c = \left\{ E \frac{3\pi}{4} \sigma_Y (COD)_c \right\}^{1/2} \qquad (14)$$

or

$$K_c = \{EG_c\}^{1/2} \qquad (15)$$

K_c is known as the fracture toughness and is a function of metallurgical and environmental (strain rate, temperature) variables through their effect on $(COD)_c$.[7]

The fracture strength σ_F of a cracked part may then easily be determined from Equation (9)

$$\sigma_F = \frac{K_c}{\sqrt{\pi a}\, f(g)} \qquad (16)$$

while the critical flaw size for unstable fracture under a tensile stress σ is:

$$a_c = \frac{1}{\pi} \left[\left(\frac{K_c}{\sigma} \right) \frac{1}{f(g)} \right]^2 \qquad (17)$$

The lifetime of a structural component t_f is the time required for a crack to nucleate (by fatigue, reactive environments, etc.) and grow slowly and stably out to the size a_c, as determined by Equation (17).

The rate of slow crack growth is a complicated function of the stress intensity factor K. For environmentally induced cracking, it has recently been established that three stages exist (Fig. 2)[8,9]

I) Essentially no crack growth occurs below a threshold value, K_o. Above K_o, the crack growth rate increases very rapidly with K;

II) A plateau region where da/dt is essentially independent of K or varies slowly with K;

III) A region of combined environmental and mechanical cracking which occurs rapidly until failure occurs at K_c.

Similar observations have been made for fatigue loading,[10,11] although da/dN does not level off completely in region II, but does show a lower dependence on K than in either regions I or III, (Fig. 3). Various analytic expressions have been proposed to compute structural lifetime. In the simplest model $K_o = 0$ and

$$\frac{da}{dn} = A(\Delta K)^n \tag{18}$$

where ΔK is the stress intensity range (i.e., $\Delta\sigma\sqrt{\pi a}$). If tension-tension fatigue is conducted with $\sigma_{MIN} = 0$, then $\Delta\sigma = \sigma$, $\Delta K = K$. Taking $n = 4$, we have

$$\frac{da}{dn} = AK^4 = A\sigma^4 \pi^2 a^2 \tag{19}$$

The lifetime may now be computed from the time required for an initial flaw of size a_i to grow out to a_c.

$$\int_{a_i}^{a_c} \frac{da}{a^2} = A\,\sigma^4\pi^2 \int_0^{N_f} dn \tag{20}$$

$$\frac{1}{a_i} - \frac{1}{a_c} = A\,\sigma^4\,\pi^2\,n_f \tag{21}$$

Combining Equations (21) and (17), with $f(g) = 1$, we have

$$n_f = \frac{1}{A\sigma^4\pi^2}\left(\frac{1}{a_i} - \frac{\pi\sigma^2}{K_c^2}\right) \tag{22}$$

This equation is often written in terms of the initial stress intensity factor of the flaw,

$$K_i = \sigma\sqrt{\pi a_i} \tag{23}$$

as

$$n_f = \frac{1}{A\sigma^2\pi}\left(\frac{1}{K_i^2} - \frac{1}{K_c^2}\right) \tag{24}$$

Consequently, it is possible to predict the lifetime of a cracked part if the initial stress intensity factor can be determined and the other parameters are known. It is in this realm that acoustic emission testing offers its greatest advantages, as discussed below.

III. Elements of Acoustic Emission Testing

Acoustic emissions are the stress waves spontaneously generated within the volume of a material that is being deformed. In the most common commercial systems used today (e.g. Dunegan Corporation 3000 Series) the emissions are detected by coupling a PZT sensor directly to the specimen or structure under load. The transducer signals are preamplified and filtered before being inserted into a secondary amplifier and filter. The amplified and filtered signals are then fed into a counter which counts the number of times the signal exceeds a certain threshold level for triggering the counter.

As discussed by Harris et al.,[13] the signals consist of damped sinusoids with a frequency corresponding approximately to the resonant frequency of the transducer, as shown schematically in Figure 4. A given acoustic emission event within the structure does not produce a single count, but rather produces several counts associated with the number of times the signal crosses the threshold V_t in "ringing down" to a voltage below the trigger level. Three counts would result from the signal shown schematically in Figure 4. Larger events produce more signals in ringing down to a voltage below the trigger level. Consequently the number of counts is a function of the energy released in the event, ΔE_g.

Harris et al.,[13] have proposed that the initial voltage output from the transducer V_o, is proportional to the square root of the energy released during a given deformation process.

$$V_o = \psi \sqrt{\Delta E_g} \tag{25}$$

They have also shown that the number of "counts" n associated with the dampled sinusoid is

$$n = \frac{f}{\beta} \ln\left(\frac{V_o}{V_t}\right) \tag{26}$$

where f = linear frequency, β = damping constant, and V_t is the threshold voltage. Combining Equations(25) and (26) gives

$$n = \frac{f}{2\beta} \ln\left(\frac{\psi^2(\Delta E_g)}{V_t^2}\right) \tag{27}$$

Acoustic emissions are produced by a variety of processes. The two that are of principal concern here are

1) plastic deformation

2) cracking (both microcracking and macrocrack growth).

The emissions that occur at the tip of a macrocrack result from plastic deformation in the plastic zone, or slow crack growth, or both of those processes and therefore can be used to characterize the K factor of the crack.

The relaxation process (ΔE_g) that produces some acoustic emission counts is a function of a deformation variable, such as stress or strain in a tensile test conducted on flaw free materials or K in a fracture mechanics test of a cracked specimen. Let us denote this variable as x, such that

$$n = n(x) \tag{28}$$

The number of events ρ that occur during deformation or fracture is rarely a constant, but is also a function of the deformation state. Thus

$$\rho = \rho(x) \tag{29}$$

Let N(x) be the total number of counts that will have occurred after a material has reached a deformation state x. N(x) will be a function both of the number of counts per event and the number of events that will have occurred.

$$N(x) = \int n(x)d\rho = \int n(x)\left(\frac{d\rho}{dx}\right)dx \tag{30}$$

then

$$dN = n(x)\frac{d\rho}{dx}\,dx \tag{31}$$

and thus the count rate dN/dt is

$$\frac{dN}{dt} = n(x)\left(\frac{d\rho}{dx}\right)\left(\frac{dx}{dt}\right) \tag{32}$$

For example the count rate that is measured during a uniaxial tensile test conducted at an (essentially) constant strain rate ($d\varepsilon/dt$) is

$$\frac{dN}{dt} = n(\varepsilon)\left(\frac{d\rho}{d\varepsilon}\right)\left(\frac{d\varepsilon}{dt}\right) \tag{33}$$

where $n(\epsilon)$ is the number of counts that occur per deformation event, and $(d\rho/d\epsilon)$ is the density of deformation events per unit of strain. Note that if $(d\rho/d\epsilon)$ is also a function of strain rate, dN/dt will not increase linearly with $d\epsilon/dt$.

The count rate measured during the growth of a crack due to stress corrosion cracking is

$$\frac{dN}{dt} = \left(\frac{dN}{dA}\right)\left(\frac{dA}{dt}\right) \tag{34}$$

where A is the area swept out by the growing crack and dA/dt is the areal rate of crack growth. For the linear growth of a through-thickness crack

$$A = Ba$$

$$dA = Bda$$

so

$$\frac{dN}{dt} = \left(\frac{dN}{da}\right)\left(\frac{da}{dt}\right) \tag{35}$$

The separation of dN/da into two parameters as in Equation (33) is presented in Section VI.

It has been noted that when hydrogen cracking occurs in cathodically charged 4340 steel, (da/dt) is proportional to K and dN/dA is proportional to K^4. Consequently, dN/dt is proportional to K^5 and small changes in K lead to rapid increases in count rate.[14] In this manner, it is possible to associate a critical count rate with a critical K value, (K_c), and hence with the onset of failure. As shown in Figure 5, the count rate on four cathodically charged bolts approached the critical value associated with K_c, as predicted from independent tests (on DCB specimens) of dN/dt - K relationships. Thus, it is not necessary to determine total counts to predict the onset of failure. In fact, in most applications, dN/dt provides a more sensitive measure of K.

IV. Processes Leading to Acoustic Emission

Acoustic emissions result from various processes of deformation and fracture which release energy that is transmitted to the transducer mounted on the specimen or structural component. In order to further develop AET methods, it is necessary to relate microscopic processes of flow and fracture to $n(x)$ and $\rho(x)$. Equation (27) shows that $n(x)$ is a function of the energy released per event, ΔE_g. Consequently, it is necessary to determine relationships between ΔE_g and deformation processes that are functions of σ, ε, K, etc. As a first approximation, we have

$$\Delta E_g = (w)(v)\lambda \tag{36}$$

w is the strain energy released per event per unit volume

v is the volume being relaxed

λ is a parameter that measures the attenuation and dissipation of sonic waves prior to their arrival at the transducer. Little is known about this parameter and for purposes of subsequent discussion we will take $\lambda = 1$ although this is certainly a gross assumption.

The value of ΔE_g will then depend on w and v. For purposes of subsequent discussion we assume a rectangular cross section of width W, thickness B and, for uniaxial tensile loading, a gage length ℓ. We also assume that the material is composed of cubical grains of size d.

Various processes of deformation and fracture produce various values of w and v. For example, the brittle fracture of a tensile bar at stress level $\sigma = \sigma_F$ has

$$\begin{aligned} w &= \sigma_F^2/2E \\ v &= BW\ell \\ \Delta E_g &= (\sigma_F^2/2E)(BW\ell) \end{aligned} \tag{37}$$

and the number of counts $n(\sigma)$ resulting from this one event ($\rho = 1$) is extremely large.

Alternately, the cleavage of one grain alone (i.e., a microcrack is formed but is blocked by grain boundaries) will relax the stress σ only over a volume of the order of d^3, so that

$$\Delta E_g \cong \left(\frac{\sigma^2}{2E}\right) d^3 \tag{38}$$

for B=W=1 cm and ℓ = 10cm, and d = 10^{-3}cm, we see that the energy released by this one event will be 10 orders of magnitude smaller than that released by the failure of the entire tensile specimen. However, since n is proportional to $\ell n(\Delta E_g)$, n will only be reduced by a factor of 10 compared with the failure of the entire specimen. Note that although stress is relaxed over the entire cleaved grain, the specimen as a whole exhibits only a miniscule load drop, since the adjacent grains immediately pick up the load that had been carried by the failed grain. The stiffness of the specimen is reduced by the order of (d^2/BW), which is too small to be detected on the conventional stress-strain curve. These events are easily detected by AET.

Similar concepts apply in the case of uniaxially loaded fiber composites.[15] Assuming a simple isostrain model where the strain ε in the fiber and the composite is identical, and the fiber remains elastic until fracture, then $\sigma = E\varepsilon$.

$$\Delta E_g = \left(\frac{\sigma^2}{2E}\right) d^2 \ \frac{\ell_c}{4} \tag{39}$$

The energy released by a fiber that breaks at a strain (composite strain) ε is then

$$\Delta E_g = \frac{\varepsilon^2 E}{2} \ d^2 \ \left(\frac{\ell_c}{4}\right) \tag{40}$$

where d is the fiber diameter and $\ell_c/2$ is the length of fiber over which relaxation followed by partial reloading occurs.[13]

Similarly the yield drop in one grain due to dislocation source operation at a stress σ produces an energy release

$$\Delta E_g = \left(\frac{\sigma^2 - \sigma_i^2}{2E}\right) d^3 \tag{41}$$

where σ_i is the friction stress level required to move dislocations through the grain. According to the elementary principles of dislocation theory, the yield drop $(\sigma - \sigma_i)$ that occurs when one grain "yields" results from the pile up of $\bar{n}$ dislocation of Burgers vector b against a grain boundary.

$$(\sigma - \sigma_i) \cong \left(\frac{\bar{n}b}{d}\right) E \tag{42}$$

The yield drop occurs at a fixed strain ε_A where

$$\varepsilon_A = \frac{\sigma}{E} \tag{43}$$

a portion of the strain is converted into a plastic component

$$\varepsilon_p = \frac{\bar{n}b}{d} \tag{44}$$

while the elastic component is reduced from ε_A to

$$\varepsilon_E = \frac{\sigma_i}{E} \tag{45}$$

Equation (41) then becomes

$$\Delta E_g = \frac{(\sigma - \sigma_i)(\sigma + \sigma_i)}{2E}\, d^3 = \frac{\bar{n}b}{2}(\sigma + \sigma_i)d^2 \tag{46}$$

and for σ of the order of σ_i this becomes simply

$$\Delta E_g \cong (\bar{n}b)\, \sigma_i\, d^2 \tag{47}$$

V. Acoustic Emission and Tensile Testing

Having discussed several of the events that produce acoustic emission, it is now possible to consider some of the important aspects of the signals generated during mechanical testing.

a) Fracture of fiber composites and brittle metals during uniaxial tensile loading.

In most fiber composites, the fibers have a distribution of strengths such that the number of broken fibers increases with increasing stress acting on the fibers. Failure of the composite occurs when a microcrack generated during the breaking of a single fiber can propagate unstably through the surrounding matrix and fibers (brittle composites) or when the cross section remaining after a large number of fiber breaks have occurred is too small to carry the load and overload failure takes place (ductile composite).[16]

Harris et al.[13] have conducted a detailed study of fiber failure in the ductile eutectic composite Aℓ-$Aℓ_3Ni$, which provides an example of the second case. The density of broken fibers observed metallographically was shown to follow a distribution that is similar to the Weibull distribution:

$$\rho(\epsilon) = a(1 - \ell^{-b\epsilon^c}) \tag{48}$$

In this material a and b and c are such that only a small fraction of the total fiber population will fail prior to the final failure of the composite. It should be noted that the composite strain and fiber strain are equal in uniaxially alligned composites and that $\epsilon = \sigma/E$. Since fiber failure is believed to occur at a critical stress,[16] the observed distribution probably

results from a true distribution of the form

$$\rho(\sigma) = a\left(1 - \ell^{-b\left(\frac{\sigma}{E}\right)^{c}}\right) \tag{49}$$

However, it is more convenient to treat composite strain rather than fiber stress as the independent test variable, and this is the procedure that was used by Harris et al.[13] With ΔE_g given by Equation (40), and n given by Equation (27), then

$$n(\varepsilon) = C\ \ell n\left(\frac{\varepsilon}{\varepsilon_0}\right) \tag{50}$$

where ε_0 is the strain corresponding to the threshold condition such that the transducer can be activated. The total number of counts is then easily obtained by differentiating Equation (48) to determine $(d\rho/d\varepsilon)$

$$\frac{d\rho}{d\varepsilon} = \frac{abc\ell^{-b\varepsilon^{c}}}{\varepsilon^{1-c}} \tag{51}$$

and inserting into Equation (30)

$$N(\varepsilon) = C\int_{\varepsilon_0}^{\varepsilon} abc\ \frac{\ell^{-b\varepsilon^{c}}}{\varepsilon^{1-c}}\ \ell n\left(\frac{\varepsilon}{\varepsilon_0}\right) d\varepsilon \tag{52}$$

Figure 6 shows that the predicted number of counts is in close correspondence with the actual counts observed during acoustic emission testing. Acoustic emission testing can thus be utilized to monitor the breaking of fibers prior to the onset of failure. Alternately (AET) provides a simple technique for determining $\rho(\varepsilon)$ without recourse to the tedious task of metallographically counting the cracked fibers.

(AET) is irreversible. Suppose a composite is loaded to a certain strain ε_1, and $N(\varepsilon_1)$ counts have been emitted from $\rho(\varepsilon_1)$ broken fibers. If

the composite is unloaded and then reloaded, no emission will be observed until $\varepsilon > \varepsilon_1$ and stronger fibers begin to break. Thus, (AET) can be used to provide a measure of damage in a material (i.e., the peak strain or peak pressure that has been applied to a well characterized material). This is the basis for the Passive Pressure Transducer[17] which can accurately measure peak pressure by passive techniques. Figure 7 shows an application of this technique to record peak impulse during the plate slap test of a composite material. Following plate slap (which produces fiber cracking), the composite is tested in a tension or bend test and acoustic emission counts are recorded. Increasing peak impulse causes increasing fiber cracking and decreases the noise that is subsequently recorded at a given stress level (or increases the applied stress required to produce a given dN/dt). (AET) can thus be used to determine the peak impulse that was applied to a well characterized composite.

In the Aℓ-$Aℓ_3Ni$ system the number of events which produce emission increases slowly with applied strain (Eq. 51) until failure occurs. However, this is not always the case. In low carbon steel the density of non-propagating microcracks varies with stress σ as[19]

$$\rho = (\sigma/\sigma_o)^9$$

$$\frac{d\rho}{d\sigma} = 9\,\frac{\sigma^8}{\sigma_o^9} \tag{53}$$

where σ_o is the stress level at which one microcrack per cm^3 has formed. The range of stress between σ_o and the fracture stress of the "composite" σ_f is relatively narrow (Figure 8) so that no acoustic emission will be observed until just prior to final failure. Note that in sharp contrast to the case of the ductile composite, the increased acoustic emission rate that would

be observed as the fracture stress is approached results from the rapid increase in the number of events, rather than in the energy released per event, which only enters the $N(\sigma)$ equation as the logarithm of $\sqrt{\Delta E_g} \propto \ell n(\sigma/\sigma_o)$. The range of stress (or strain) over which acoustic emission occurs thus provides a measure of the stress (or strain) dependence of the density of sources leading to emission.

Figure 9 is a schematic diagram of the possible variation of (dN/dt) with deformation variable (σ,ε,K etc). Case (a) represents the ductile composite. It would be relatively difficult to predict failure in this material since (dN/dt) varies slowly with ε until failure occurs and there is no sharp cut-off point that could be used as a failure indicator. Case (b) represents the low carbon steel. Here, there is a sharp increase in emission just prior to failure, but the stress range between σ_o and σ_f is so narrow that it might be difficult if not impossible to interpret the signal and shut off the test machine (or unload the structure) prior to failure. Case (c) represents the most desirable signal indicator. Here, the acoustic emission shows a sharp increase at about 70% of the failure condition, which gives the operator plenty of warning of impending failure and also time to do something about it.

b) Yielding and plastic deformation of metals during tensile testing.

Various studies of yielding and plastic deformation have been conducted during the past several years.[20,21,22] The results of these tests indicate that[21]

1) considerable acoustic emission activity occurs before the yield strength σ_Y is reached (Figure 10);

2) (dN/dt) goes through a maximum at or close to σ_y;

3) the count rate decays rapidly after the yield strength is reached;

4) not all materials are noisy-generally, (dN/dt) is high for "brittle" materials (e.g. beryllium) and low for soft, ductile materials (copper, stainless steel, etc.).

5) In a given material, (dN/dt) increases with yield strength σ_y at a given strain level.

6) Coarse grained materials emit more sound than fine grained materials.

Several attempts have been made to linearily relate dN/dt with the mobile dislocation density, Λ as given by the Gilman equation[23]

$$\Lambda = (\Lambda_0 + m_p \varepsilon_p) \ell^{-\phi \varepsilon_p} \tag{54}$$

where Λ_0 is the number of initial mobile dislocations, m_p is the multiplication factor, ε_p is the plastic strain, and $\phi = (d\sigma/d\varepsilon)/\sigma$ is a parameter that depends on the rate of strain hardening.

The principal thrust for the use of this model lies in the fact that it can accurately account for observations (2) and (3) above. However, it cannot account for (1) (e.g., Figure 10) nor, and more important, it cannot account for observations (4) and (5).

Without offering a general criticism of the Gilman model for yielding based on the dynamics of individual dislocations, we would like to offer a different interpretation based on these acoustic emission studies. First, we believe that it is unlikely that individual dislocation motions can be detected by standard acoustic emission testing techniques. Second, the motion of an individual dislocation does not lead to a release of energy

unless the stress required to start the dislocation moving past an obstacle σ_a is greater than the stress required to keep it in motion, σ_b. If we associate σ_a with the yield strength of a single crystal σ_i and σ_b as the true lattice friction stress then we should expect to detect more emission from materials such as copper with high mobile densities and low σ_b values than from beryllium with tight bending (high σ_b) and few mobile dislocations. In fact, just the reverse is noted (observation 4). Furthermore, a model based on individual dislocations cannot account for the large acoustic activity detected before yield (observation (1)), nor for the grain size dependence of dN/dt, (observation 6).

Instead, we believe that the acoustic emission bursts result from the operation of pinned dislocation sources (or the creation and operation of fresh sources)[31] and the generation of glide band packets containing $\bar{n}$ dislocations each. As shown in Equation (47), the energy released by each source operation is proporational to the lattice friction stress σ_i (in accord with observation (5)), the grain size (in accord with observation (6)), and the number of dislocations in the pile up, $\bar{n}$. This is consistent with the fact that brittle materials in which unstable plastic flow events (large pile-ups) can occur are noisier than ductile materials, which yield more homogeneously and which strain harden more rapidly (observation 4). The increase in acoustic emission in pressure vessel steels after irradiation[24] probably results from both an increase in σ_i and an increase in the number of dislocations $\bar{n}$ generated by unstable microplastic flow events.

Observations (1-3) can be accounted for by assuming that the density of sources of glide bands (dislocation packets) follows a distribution: If the Weibull distribution applies, then

$$\rho(\varepsilon) = g\left(1 - \ell^{-d(\varepsilon-\varepsilon_0)^f}\right) \tag{55}$$

$$\frac{d\rho(\varepsilon)}{d\varepsilon} = \frac{g\ell^{-d(\varepsilon-\varepsilon_0)^f}}{(\varepsilon-\varepsilon_0)^{(1-f)}}(fd) \tag{56}$$

where $\rho(\varepsilon)$ is the number of sources that will have operated after a strain $\varepsilon > \varepsilon_0$, and $(d\rho/d\varepsilon)$ is rate of source operation. It is of course possible that ρ is an independent function of stress σ rather than strain ε and this point needs experimental confirmation. This model predicts that the deviations from linearity before σ_y result from a series of discrete load drops (Figure 11) which are generally too small to be detected in the conventional tensile test. The model is an agreement with the fact that slip band sources have been observed to operate well before the yield point is reached,[25] and that at the yield point most sources will be operating. There is absolutely no reason a priori to expect that fresh sources cannot operate after yield. However, as the "easy" sources are used up, slip will tend to occur by the motion of dislocations already generated and the acoustic emission rate drops off rapidly for $\varepsilon > \varepsilon_y$. Note that this form of acoustic emission, like that of fiber cracking, is also irreversible; once a source has been used, it cannot operate again.

VI. Acoustic Emission and Fracture Testing

Having discussed the processes leading to acoustic emission and the relation between (dN/dt) and stress level σ and/or strain level ε, we are now in a position to relate (dN/dt) to K in cracked specimens. This subject has been discussed in some detail for fatigue crack growth[26,27] hydrogen cracking,[14]

fiber cracking[15] and irradiated steels[24] and only a short review of these studies will be presented. First, it should be noted that acoustic emission can occur from two entirely separate processes near the crack tip – the growth of the plastic zone R and microcracking in the process zone at the crack tip. As discussed above, the acoustic emission that occurs during plastic strain will mainly come from grains that are just undergoing yield so that most of the activity comes from a thin ring of material at the plastic-elastic interface (Figure 12). By comparing the size of the two regions and the respective energy relaxation mechanisms (Equation 41 for the plastic zone and Equation 38 for the process zone) we see that the yielding ring will emit a large number of relatively low relaxation (small ΔE_g) emissions in comparison with the small number of high energy emissions associated with grain cracking at the crack tip. Depending on the sensitivity of the transducer and amplification system, it is possible to screen out the "low-level" acoustic emission resulting from plastic deformation at the plastic zone boundary and record only the "high-level" emission from microcracking in the process zone.

Each of these processes show a separate dependence on K. The volume (area in the two dimensional case shown here) of the ring undergoing yielding at the plastic-elastic interface (and hence the source density) is proportional to R^2. In the simplest model[20] it is assumed that $n(\varepsilon)$ is constant for all sources operating in the ring and hence N is proportional to the source density (i.e., to R^2). From Equation (10) we then have

$$N(K) \cong A \left(\frac{K}{\sigma_y}\right)^m \tag{57}$$

where m=4. Experimental values between 4 and 8 have been observed for m and some recent data by Nakamura[1] can account for these variations. The low level

acoustic emission is generally very small and difficult to detect in high yield strength materials. It is most easily detected in low strength materials (K/σ_y large) which show unstable glide band formation (e.g. low carbon steel, irradiated alloy steels, etc.).

The high level acoustic emission that results from crack growth can most easily be investigated in fiber composites containing brittle fibers dispersed in a ductile matrix, particularly if the fibers exhibit a small variance in strength about a mean value of σ_f such that all events show identical ΔE_g and $n(\sigma)$ values. All the high level emission then results from fiber cracking. We have investigated the Boron/epoxy system[13] using a bend specimen designed such that the specimen thickness B increases as the crack propagates. In this "decreasing K" type specimen, it is possible to control the crack propagation process such that increased load must be applied to break each succeeding layer of fibers. Independent measurements of specimen compliance and electrical resistance can be used to determine the number of broken fibers and relate this number to the acoustic emission counts. The results showed that the total number of counts was proportional to the number of broken fibers.

The energy released in breaking one fiber is given by Equation (39). The toughness G_c is equal to ΔE_g multiplied by the number of fibers per unit area, λ. For a constant fraction of fiber breaks at the tip of an advancing crack, we would expect that the number of counts/unit area dN/dA would be proportional to $\ell n\ (\Delta E_g)$. Since $\Delta E_g = (G_c/\lambda)$, dN/dA should be proportional to $\ell n(G_c)$. Figure 13 shows that for this system, where both G_c and dN/dA varied as the crack advanced, dN/dA does increase with G_c and with the exception of the one data point at high G_c (corresponding to the apex of the specimen where data is difficult to obtain) the trend is close to being

logarithmic. Further investigation is required to prove whether the proposed relation

$$dN/dA \propto \ell n(G_c) \tag{58}$$

applies for other composites.

The high level acoustic emission observed during rising K tests on brittle and semibrittle metals where emissions result from grain cracking and/or particle cracking will be similar to that observed for fiber cracking. As K increases, the strain distribution ahead of the crack will spread outwards and an increasing number of grains in the process zone will have been brought to their failure strain (or stress). The density distribution function $\rho(K)$ and counts/event relation $n(K)$ have not yet been determined so we cannot make a prediction of the relation between N and K. The fact that high level emissions are not observed in high strength materials until $K \cong .80\ K_{Ic}$[28] would indicate that the distribution function for cracking elements is fairly narrow.

In the presence of reactive environments which lead to hydrogen embrittlement or stress corrosion cracking, slow crack growth can occur at K levels as low as $0.02\ K_{Ic}$ and high level acoustic emissions can be detected well below $0.80\ K_{Ic}$. As discussed previously, (dN/dt) depends both on (da/dt) which is a complicated function of K (Figure 4) and (dN/da) which has not been investigated in any great detail. For the case of cathodically charged specimens of 4340 steel (dN/da) is proportional to K^4 and da/dt is proportional to K in the range investigated.[14] As shown in Figure 14, the sharp increase in (dN/dt) with K results from the fact that the time between bursts of crack growth is greatly decreased with increasing K, even though the number of counts per burst $n(\Delta a)$ may be decreasing. Since the time between bursts

decreases much faster with increasing K than the crack growth rate (da/dt) increases, the extent of crack growth per burst, Δa, is smaller at the higher K levels. Following Equation (32) we write

$$\frac{dN}{dt} = n(\Delta a) \frac{d\rho}{d(\Delta a)} \left(\frac{da}{dt}\right) \tag{59}$$

$n(\Delta a)$ is proportional to $\ell n(\Delta E_g)$ which in turn is proportional to the volume of the event, i.e., to Δa. Thus, $n(\Delta a)$ will decrease logarithmically with Δa(i.e., as K increases). However, $d\rho/d(\Delta a)$ increases inversely with (Δa) (i.e., as K increases) and since the function $[\ell n(x) \frac{1}{x}]$ increases rapidly as x decreases from a large value,

$$\frac{dN}{da} = n(\Delta a) \frac{d\rho}{d(\Delta a)} \tag{60}$$

will increase rapidly with K. The shorter time between bursts associated with higher K values results from the smaller amount of hydrogen required to fracture a highly stressed grain near the crack tip as the strain in that grain increases (i.e., as K increases).

Both the low level emission from plastic flow that predominates in low strength materials and the high level emission associated with cracking in brittle materials (irrespective of strength level) are irreversible phenomena. If a structure containing a crack is loaded to K_1, unloaded, and reloaded, no emission will occur on the second load application unless $K > K_1$. Acoustic emission testing has therefore been used in conjunction with periodic proof testing to monitor whether "old" cracks have grown, or new ones have formed, since the previous proof test. The optimum time between periodic proof tests can be predicted from the rate of crack growth, as discussed elsewhere.[26,27] For example, in the method developed by Tiffany,[29] a pressure vessel or other

structural component is proof tested at a stress $\sigma_p = \alpha \sigma_w$ where $\alpha > 1$ is the proof test factor and σ_w is the peak anticipated working stress. If failure does <u>not</u> occur in the proof test, then the initial flaw size

$$a_i \leq \frac{K_{Ic}^2}{\pi(\alpha\sigma_w)^2} \tag{61}$$

so that the maximum initial stress intensity factor under service conditions is

$$K_{Ii} = \sigma_w \sqrt{\pi a_i}$$

$$(K_{Ii})^2 = \sigma_w^2 \pi\, a_i = \frac{K_{Ic}^2}{\alpha^2} \tag{62}$$

Introducing this equation into Equation (24) we find that

$$n_f = \frac{(\alpha^2 - 1)}{A\, K_{Ic}^2\, \sigma_w^2 \pi} \tag{63}$$

for those cases where $da/dn = AK^4$. Knowing the growth constant A, K_{Ic}, and σ_w, we can determine the proof factor α that must be used in the proof test such that a given number of safe cycles n_f can be guaranteed in service.

One of the principal potential uses of acoustic emission testing is to monitor periodic proof tests as the stress is raised to $(\alpha\sigma_w)$, to detect and prevent premature failure in case the flaw size a_i is sufficiently large that failure would be expected to occur in the proof test (i.e., $a_i > K_{Ic}^2/\pi(\alpha\sigma_w)^2$).

A second approach towards acoustic emission monitoring is based on the choice of a constant proof stress $\sigma_p > \sigma_w$, and the irreversible nature of acoustic emission. If fatigue occurs at the working stress, the K factor $\sigma_p \sqrt{\pi a}$ measured during proof will have increased. Equation (57) gives the number of counts measured during proof

$$N_{proof} = A\frac{\pi^2 a^2}{\sigma_y^4}(\sigma_p^4 - \sigma_w^4) \tag{64}$$

From Equation (21) we have the crack size after n cycles of fatigue:[26]

$$a = \frac{a_i}{1 - A\,\sigma_w^4 \pi^2\, n a_i} \tag{65}$$

Combining Equations (64) and (65) we find that the number of counts measured during the proof test is

$$N_{proof} = \frac{A\,\pi^2\, a_i^2(\sigma_p^4 - \sigma_w^4)}{\sigma_Y^4[1-A\,\sigma_w^4\pi^2 n a_i]^2} \tag{66}$$

for the fatigue crack growth rate and the acoustic emission rate both varying as K^4. Similar equations can be derived for different functional relations between N(K) and da/dn. Figure (15) shows that this approach is in excellent agreement with experimental data on trip steel. Consequently a sharp increase in acoustic emission during proof test can be used to indicate that failure is about to occur (i.e., that $N(K) \to N_c$, or $dn/dt \to (dn/dt)_c$). The use of acoustic emission testing to monitor crack growth in chemical and nuclear pressure vessels has developed rapidly in the past few years and undoubtedly will continue to do so.

The extreme sensitivity of (AET) to slow crack growth processes in reactive environments means that susceptibility to stress corrosion cracking can be quickly and easily determined by placing pre-cracked, pre-loaded specimens of questionable microstructure or composition in known solutions and measuring dN/dt. As shown in Figure (16), the rapid emission from alloy A indicates that it is considerably more sensitive to SCC than B or C in this particular solution.

VII Conclusions

Acoustic Emission testing has found many uses in recent years and new applications are constantly being uncovered. One of the most fruitful areas for application lies in the characterization of microscopic processes of yielding and fracture, and macroscopic processes of slow crack growth and onset of fast crack propagation. This paper has described these processes and emphasized that the total counts and count rate depend on the energy released per event and the density of events per unit of deformation. The models presented herein are first order approximations which await confirmation.

VIII Acknowledgments

The author wishes to thank Dr. D. Harris and Dr. K. Ono for reading the manuscript and making valuable suggestions. Support for fracture mechanics programs at UCLA is provided through AROD Contract DAH-04-68-0008 and this continuing support is gratefully acknowledged.

References

1. Acoustic Emission Testing, ASTM STP #505, published by ASTM, Philadelphia, May 1972.

2. Materials Research & Standards, Vol. 11, No. 3, (1968).

3. F.A. McClintock and G.R. Irwin, Fracture Toughness Testing, ASTM Philadelphia, STP 381 (1965) p. 84.

4. J.F. Knott and A.H. Cottrell, J.I.S.I., 201, 249 (1963).

5. T.R. Wilshaw, C.A. Rau, and A.S. Tetelman, Engineering Fracture Mechanics, 1, 191 (1968).

6. P. Paris and G. Sih, Fracture Toughness Testing, ibid, p. 30.

7. A.S. Tetelman and A.J. McEvily, Fracture of Structural Materials, Wiley, New York (1967).

8. A. Evans, to be published in Int. J. Frac. Mechanics.

9. S. Wiederhorn, J. Am. Ceram. Soc., 50, 407 (1967).

10. D. Williams, to be published.

11. A.J. McEvily et al., presented at Fourth National Symp. on Fracture Mechanics, Carnegie-Mellon University (1970).

12. P. Paris, Proc. Tenth Sagamore Army Mat. Res. Conf., Syracuse Univ. Press (1963).

13. D. Harris, A.S. Tetelman, and F. Darwish, Acoustic Emission Testing ibid.

14. H. Dunegan and A.S. Tetelman, Engineering Fracture Mechanics, 2, 387 (1971).

15. J. Fitz-Randolph, et al., J. Composite Materials, 5, 542 (1971).

16. A.S. Tetelman, Composite Materials, Testing and Design, ASTM STP 460, p. 473 (1969).

17. Dunegan Corporation, Livermore, California.

18. F. Tuler, Effects Technology Corporation Rept. TR 70-01 (December 1970).

19. L. Kaechele and A.S. Tetelman, Acta Met., 17, 463 (1969).

20. H.L. Dunegan, D. Harris, C. Tatro, Eng. Fracture Mechanics, 1, 105 (1968).

21. H.L. Dunegan and A.T. Green, Mat. Res. & Stds., 11, No. 3, p. 21, (1968).

22. W. Gerberich and W. Reuter, Final Rept. to ONR, Contract No. 00014-66-60340, (1969).

23. J. Gilman, Proc. 5th U.S. Nat. Cong. Appl. Mech., N.Y. 1966 p. 385.

24. D. Ireland et al., Conn. Yankee Reactor Vessel Survellance Program Report, Battelle, Columbus, Ohio (1970).

25. J. Suits, and J.R. Low, Jr., Acta Met., 5, 285 (1957).

26. H.L. Dunegan, D.O. Harris, and A.S. Tetelman, Mat'ls. Evaluation, p. 221 (1970).

27. D. Harris, H.L. Dunegan, A.S. Tetelman, Proc. A.F. Conf. on Fatigue and Fracture, AFFDL TR 70-144 (1970) p. 459.

28. P.G. Bentley, et al., presented at Inst. of Mech. Eng. Conf. on Acoustic Emission, March (1972).

29. C.F. Tiffany and J.N. Masters, Fracture Toughness Testing, ibid. p. 249.

30. A.S. Tetelman and H.L. Dunegan, Research/Development, May 1971, p. 21.

31. D. James and S. Carpenter, J. Appl. Phys., 42, 4685 (1971).

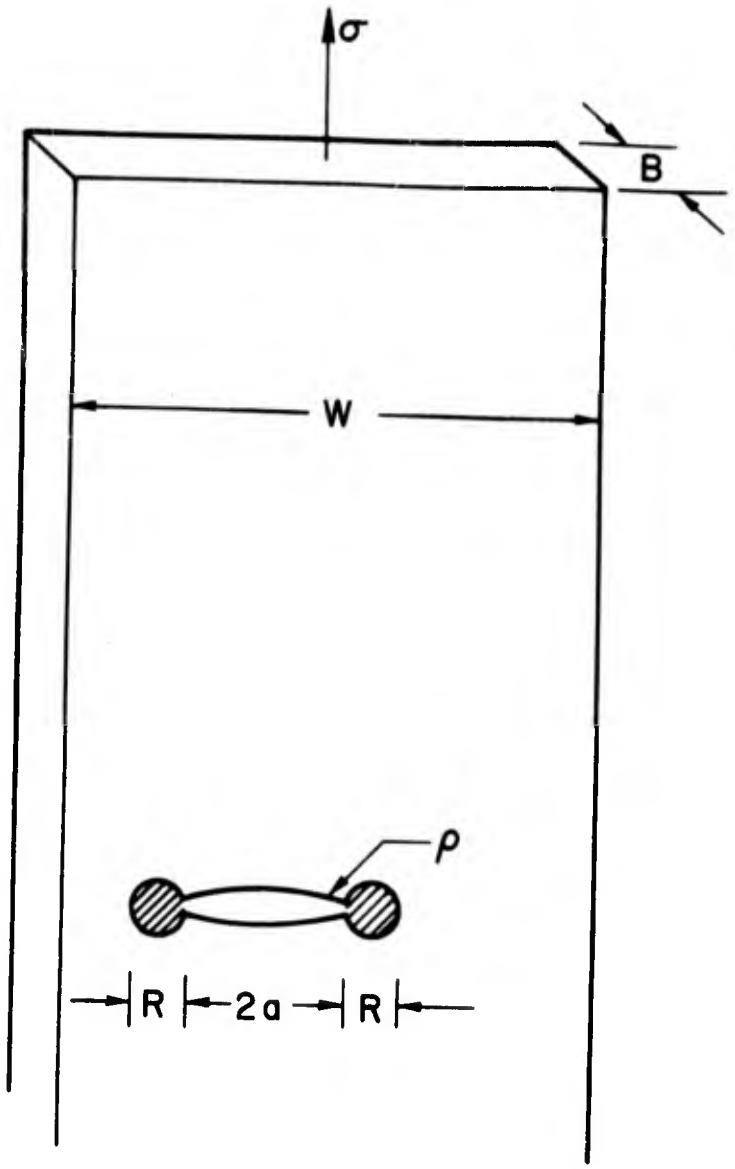

Figure 1. Formation of Plastic Zone in a Cracked Plate

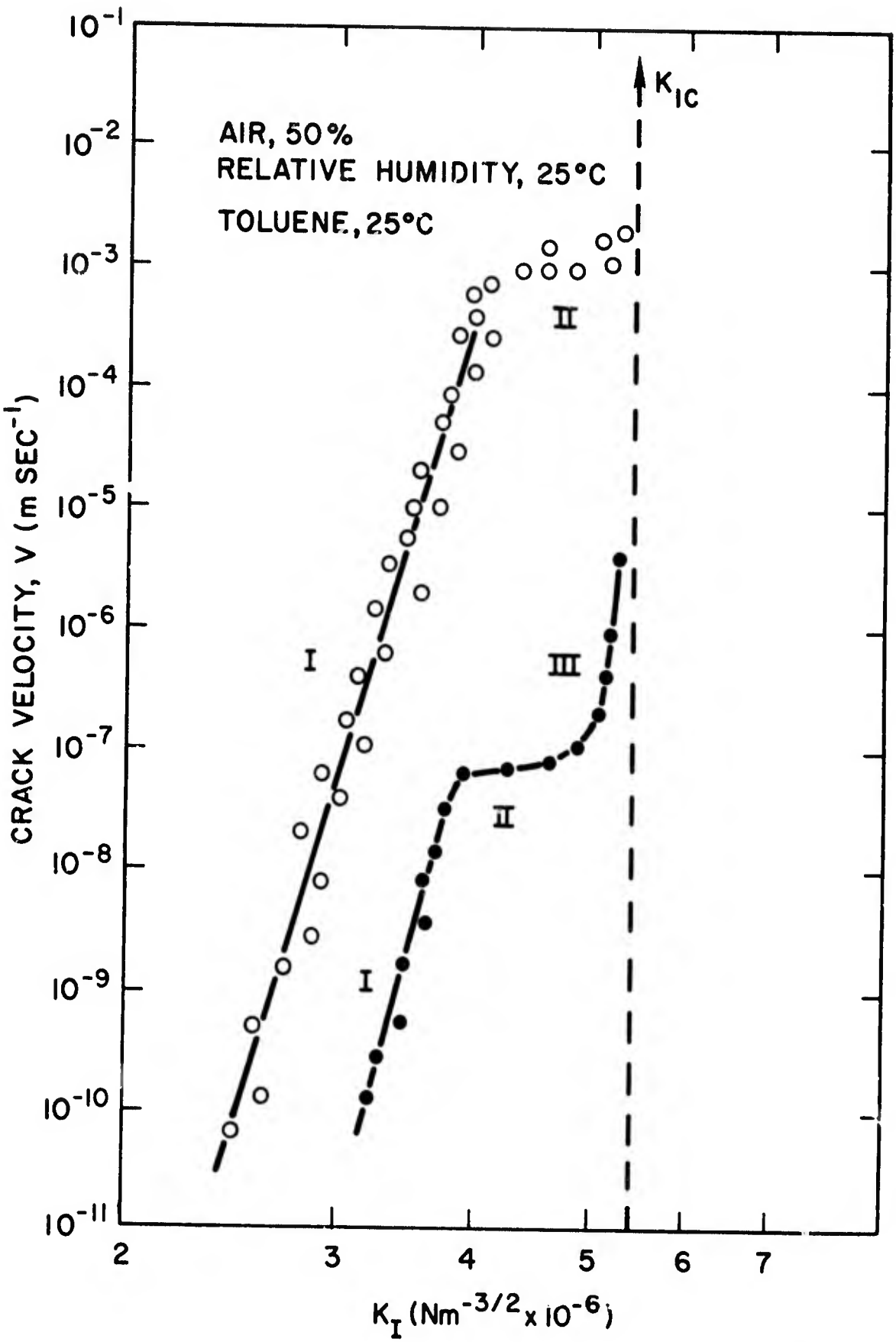

Figure 2. Effect of K on Crack Velocity in Glass in Air and Toluene (Courtesy T. Evans[8])

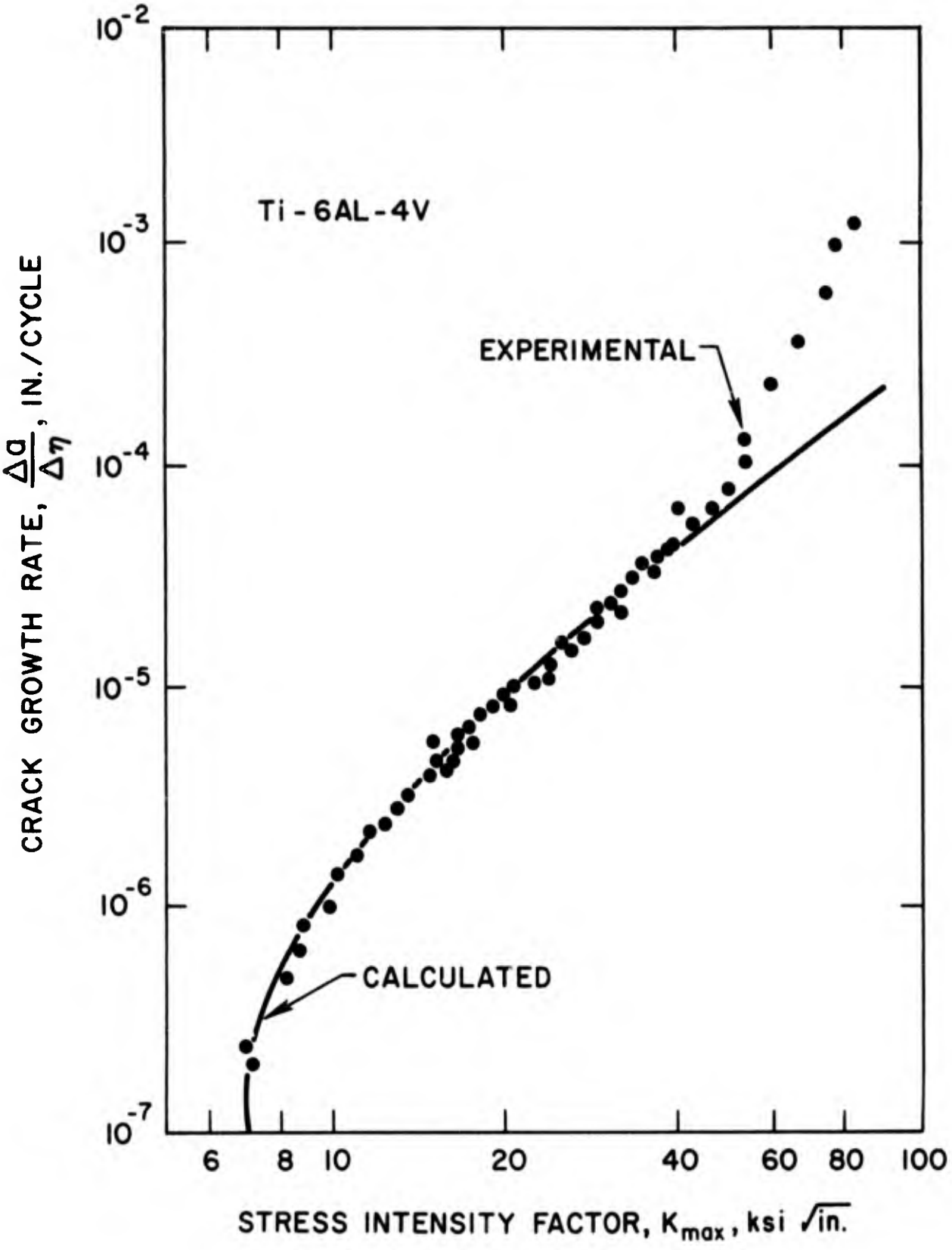

Figure 3. Effect of K_{max} on Crack Growth Rate in Ti 6Aℓ-4V. (After A. McEvily et al.,[11])

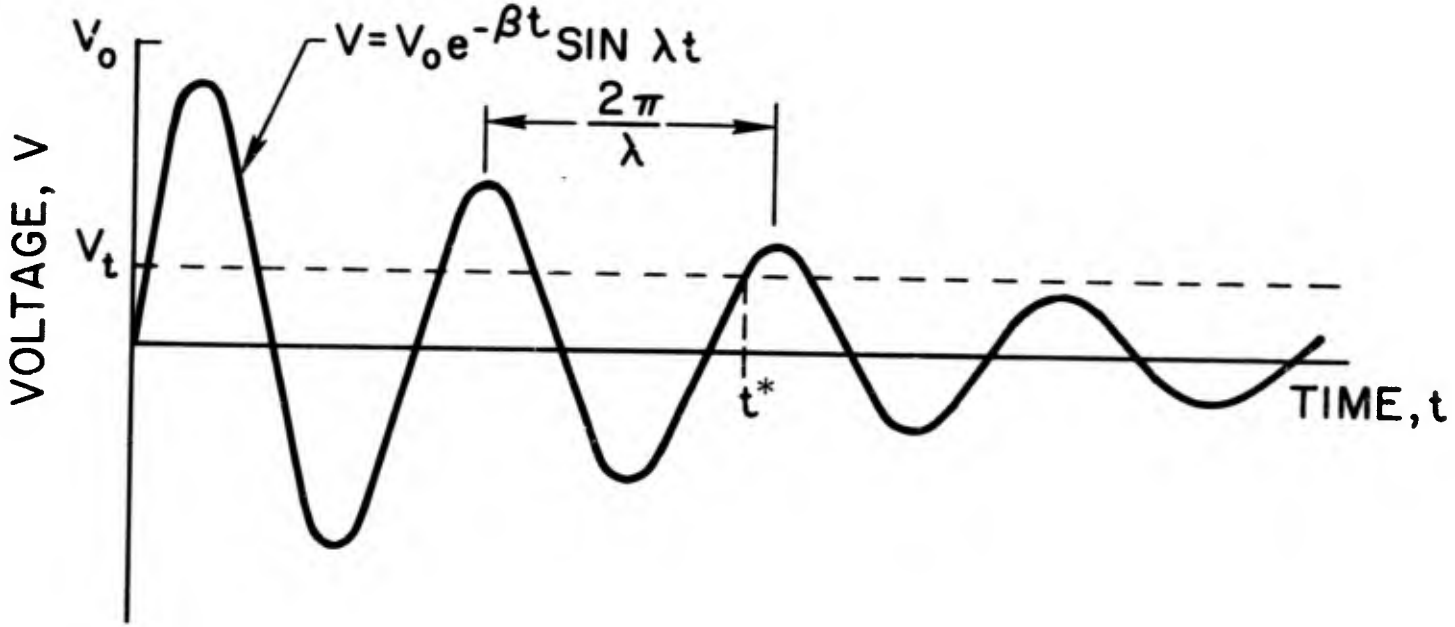

Figure 4. Schematic of a Damped Sinusoid Signal, showing Threshold Voltage, and the Multiple Counts Resulting from a Single Event within the test piece.(13)

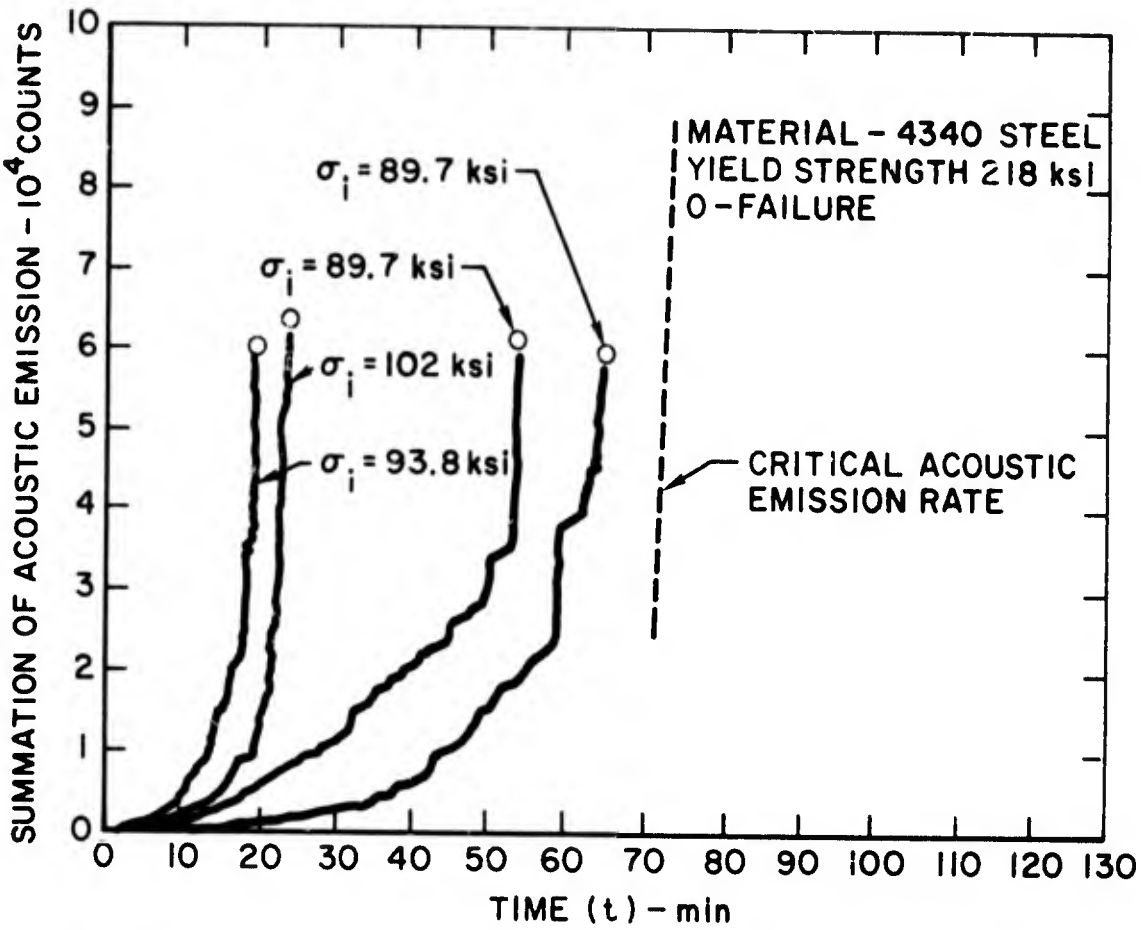

Figure 5. Summation of Acoustic Emission over a Period of Time t for Cathodically Charged and Torqued Bolts of 4340 Steel. Failure Predicted to Occur at the Critical Count Rate shown by the dotted line. After H. Dunegan and A.S. Tetelman[14]

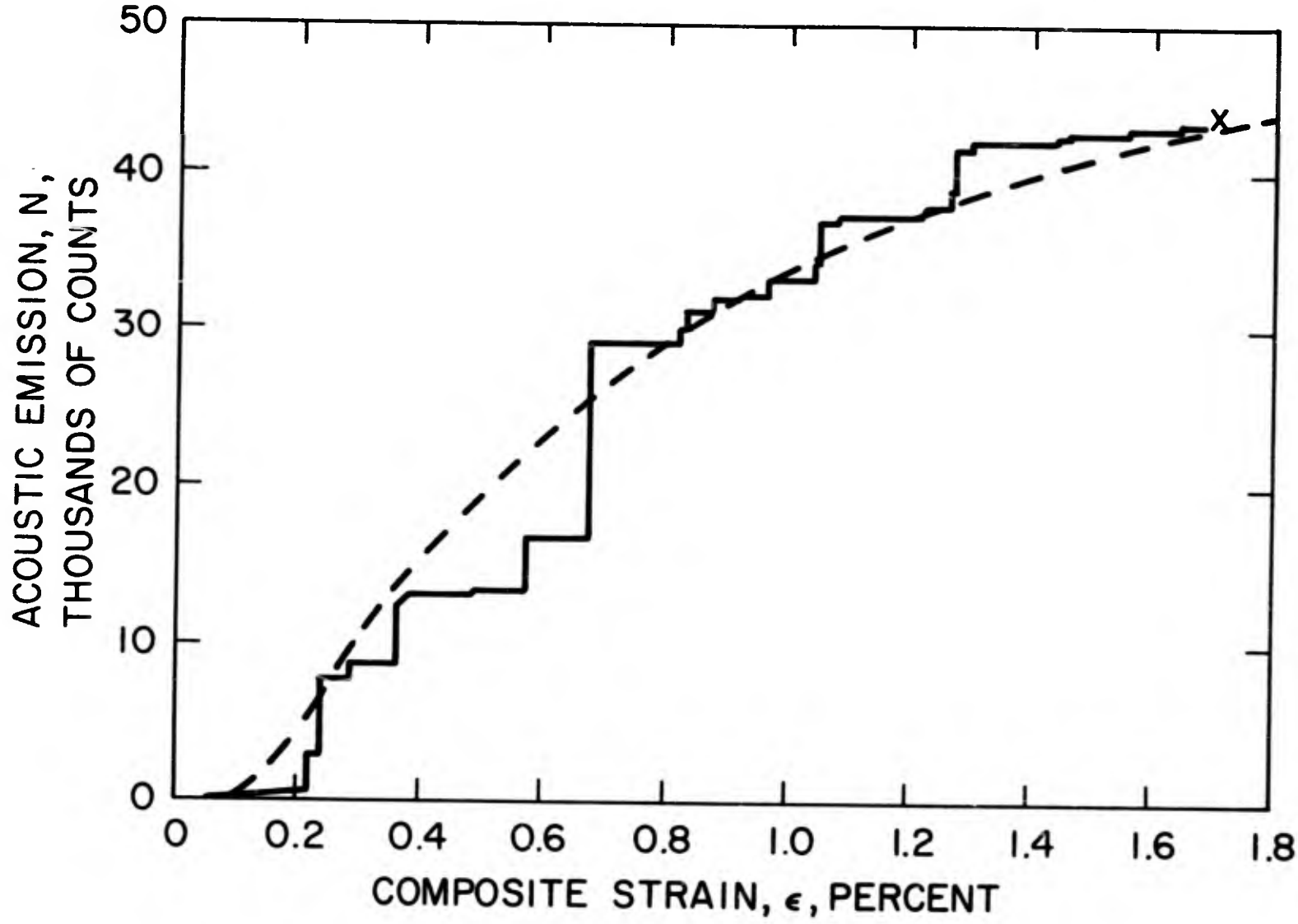

Figure 6. Results of Theoretical Calculations of Summation of Acoustic Emission as a Function of Strain. Experimental Results for Aℓ-$Aℓ_3Ni$ are also Included[11]

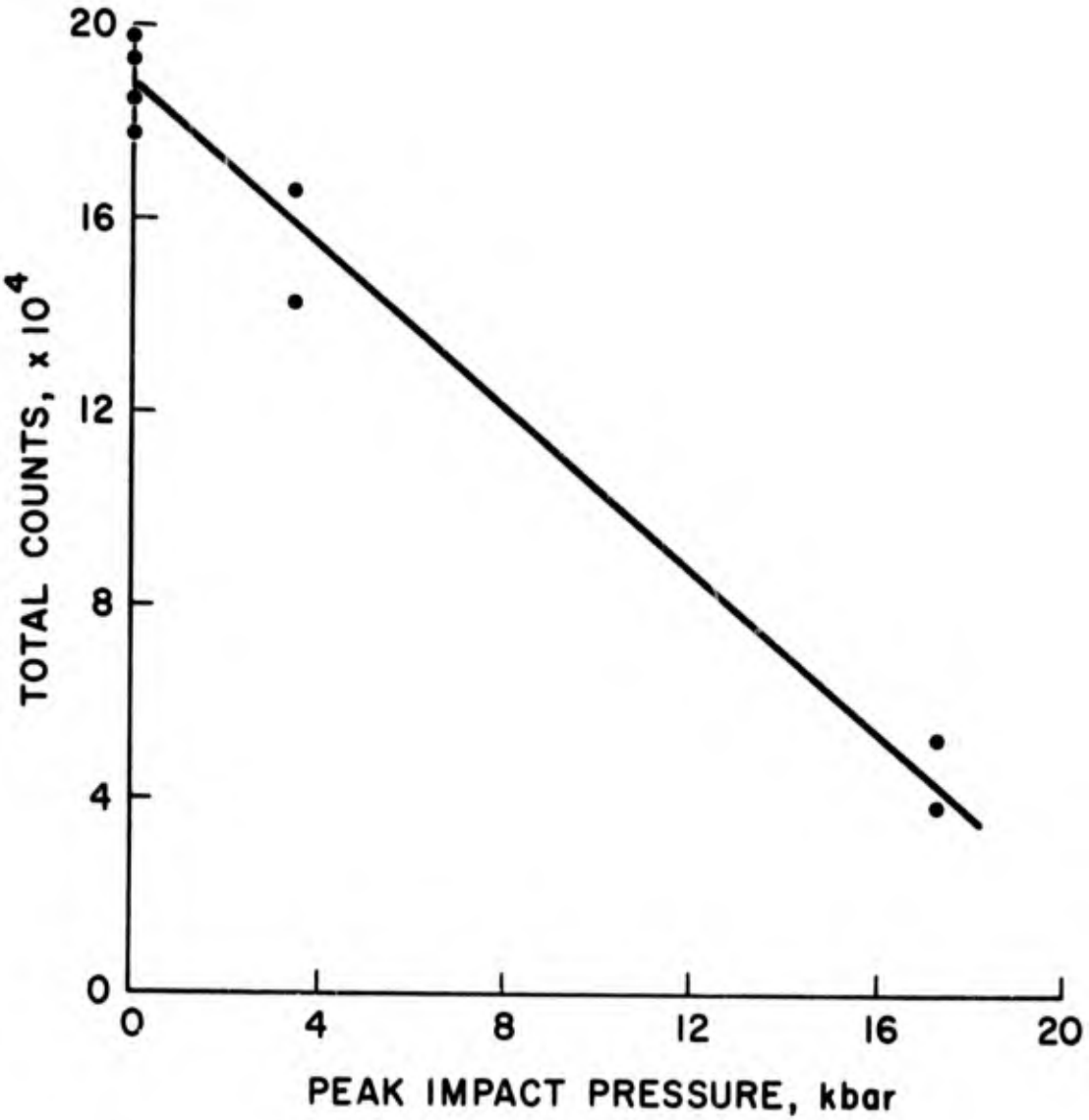

Figure 7. Total Acoustic Emission Counts at Failure as a Function of Peak Impact Pressure for 0° Lay-up Carbon Phenolic (after Tuler[18])

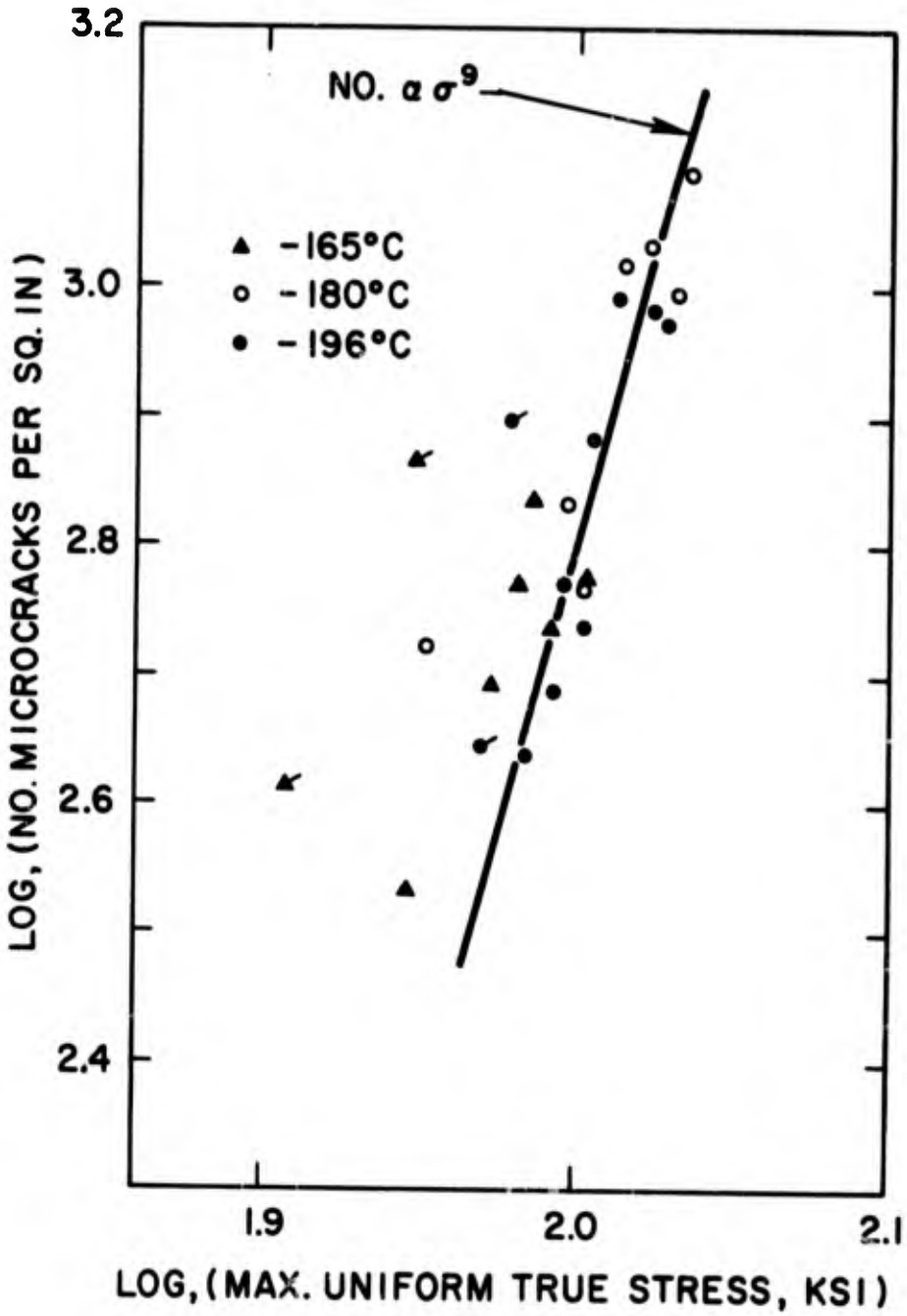

Figure 8. Stress Dependence of Microcrack Formation in Low-Carbon Steel Tension Specimens (after L. Kaechele and A.S. Tetelman).[19]

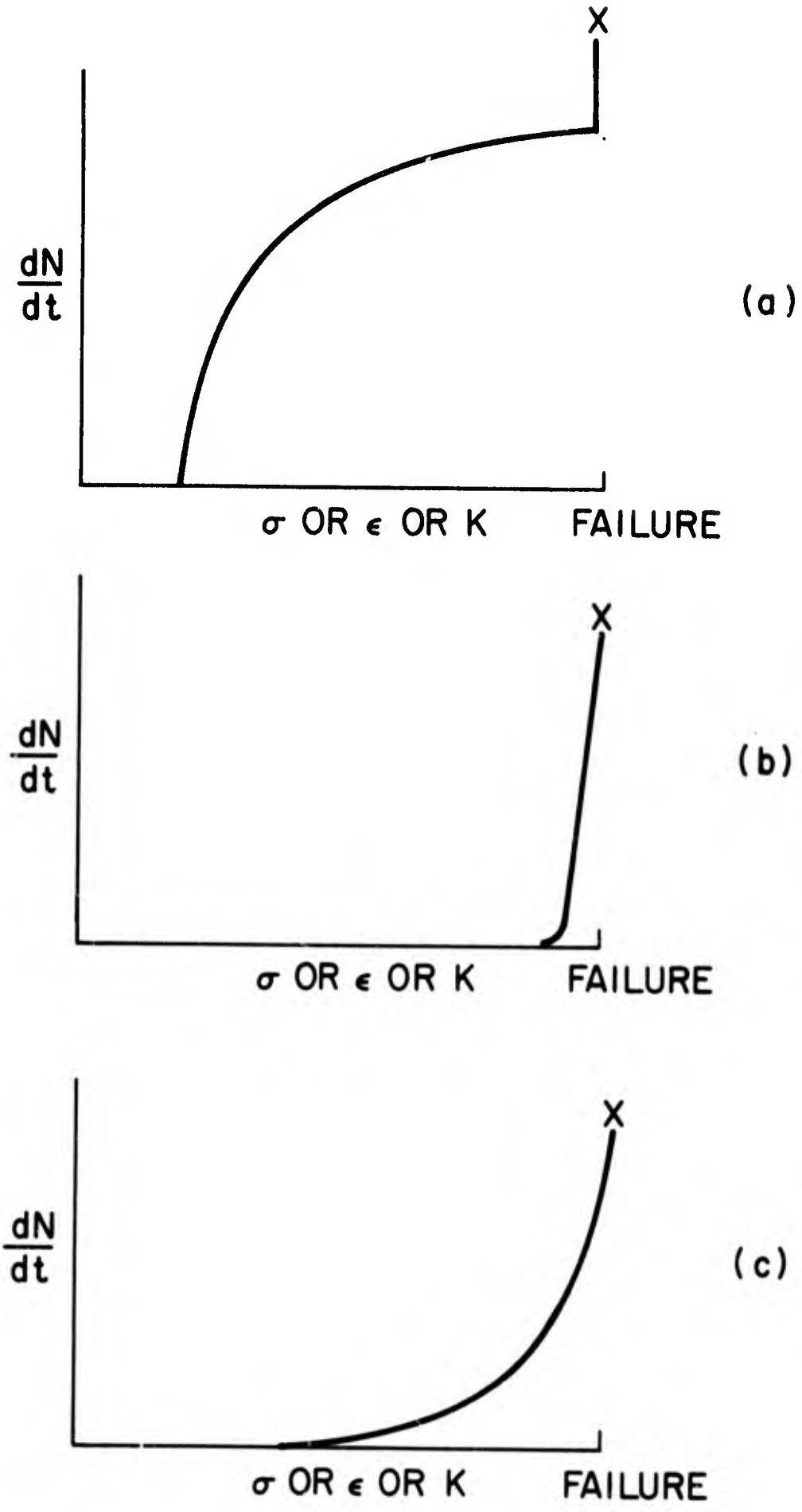

Figure 9. Possible Variations of $\frac{dN}{dt}$ with Deformation Variable. Case (C) is Most Desirable for Purposes of Failure Detection

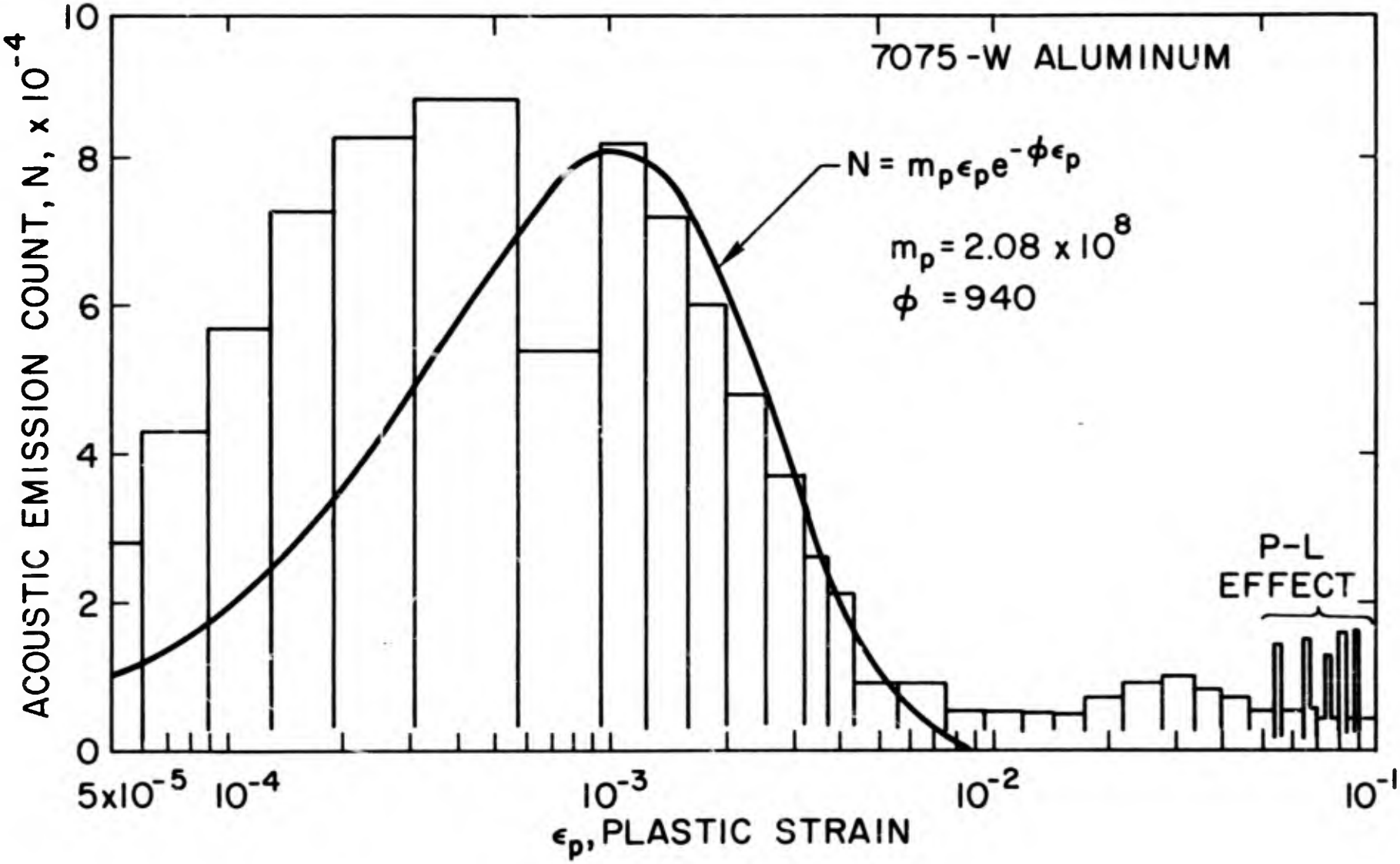

Figure 10. Fit of Dislocation Mobility Model to Acoustic Emission Data for as-Quenched 7075 Aluminum (after W. Gerberich and W. Reuter).[22]

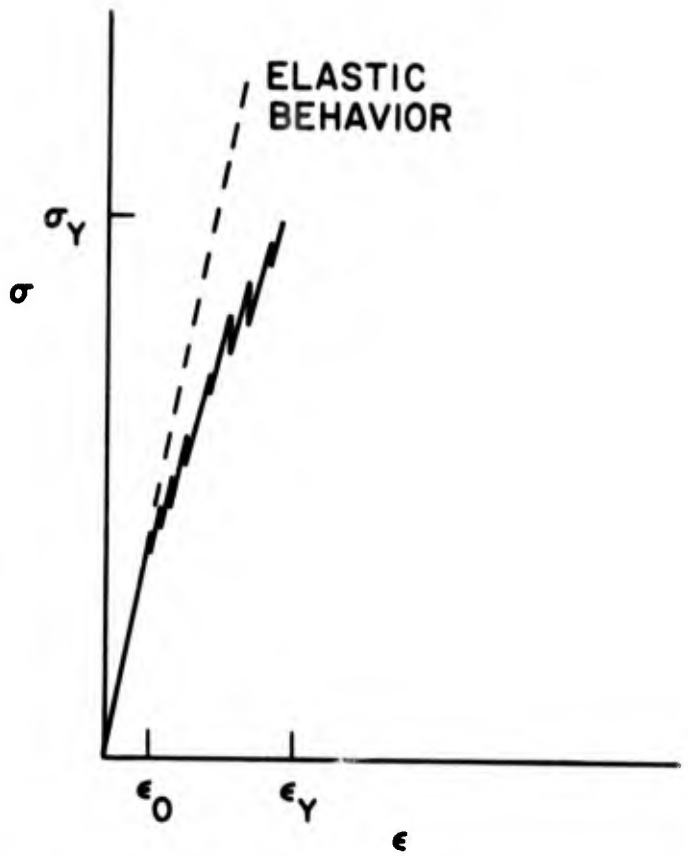

Figure 11. Microyielding and Deviations from Elastic Behavior Shown as a Series of Microyield Drops

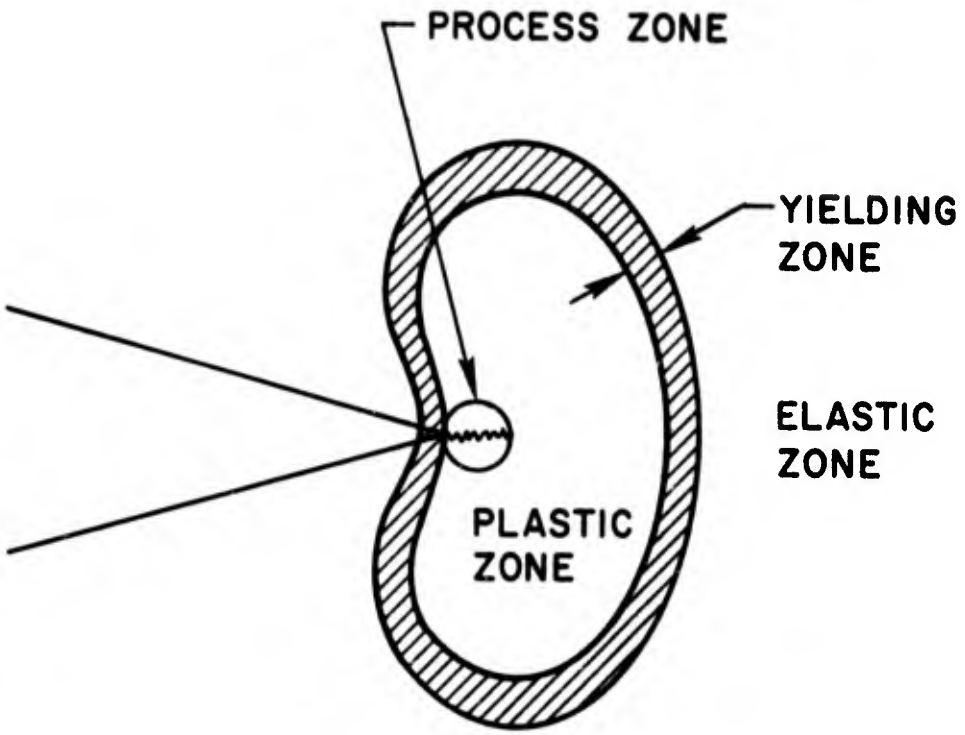

Figure 12. Zones Producing Acoustic Emission near Crack Tip

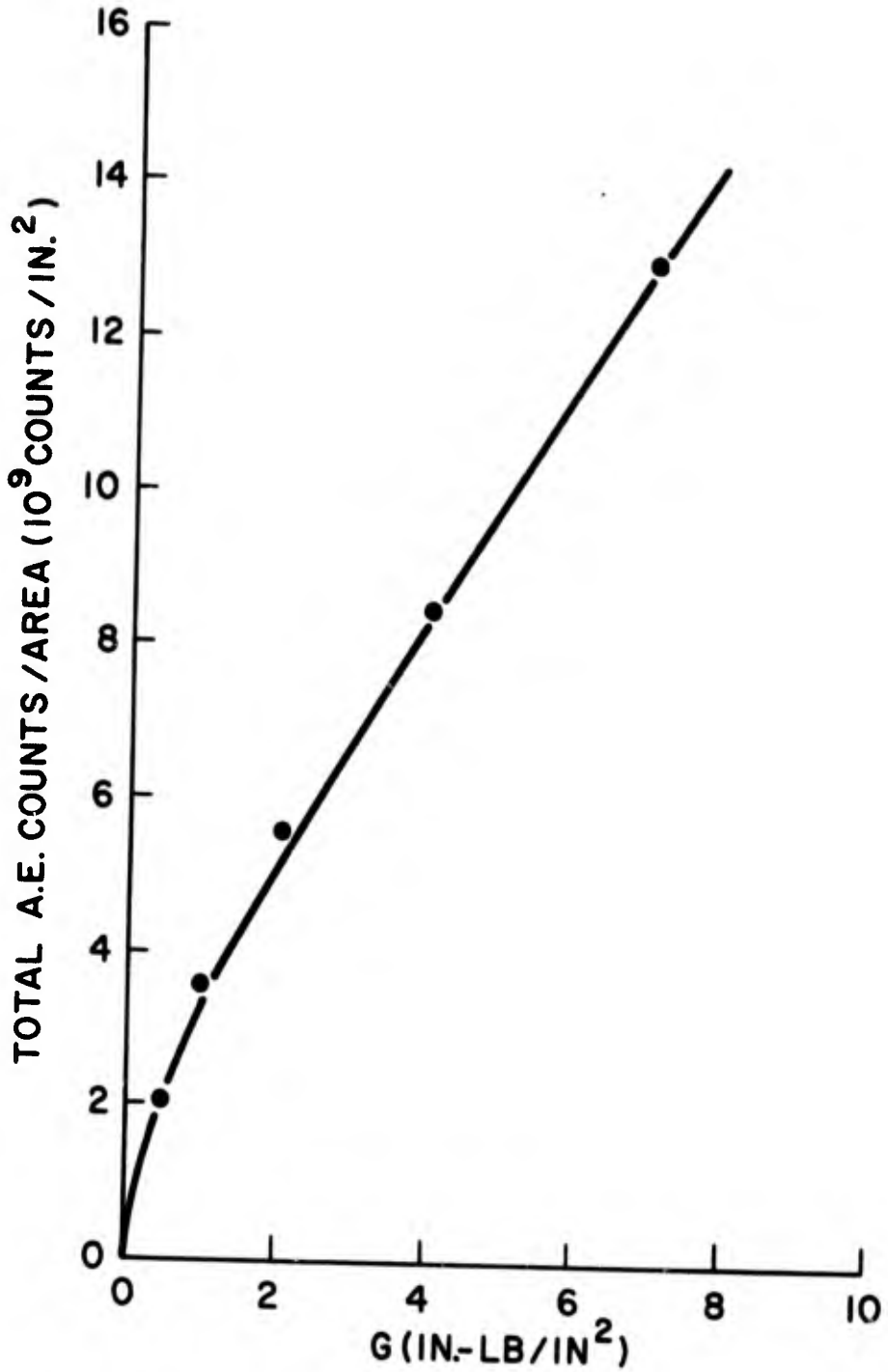

Figure 13. Variation of Total A.E./Area with G for Type A Roof-Top Specimen(15)

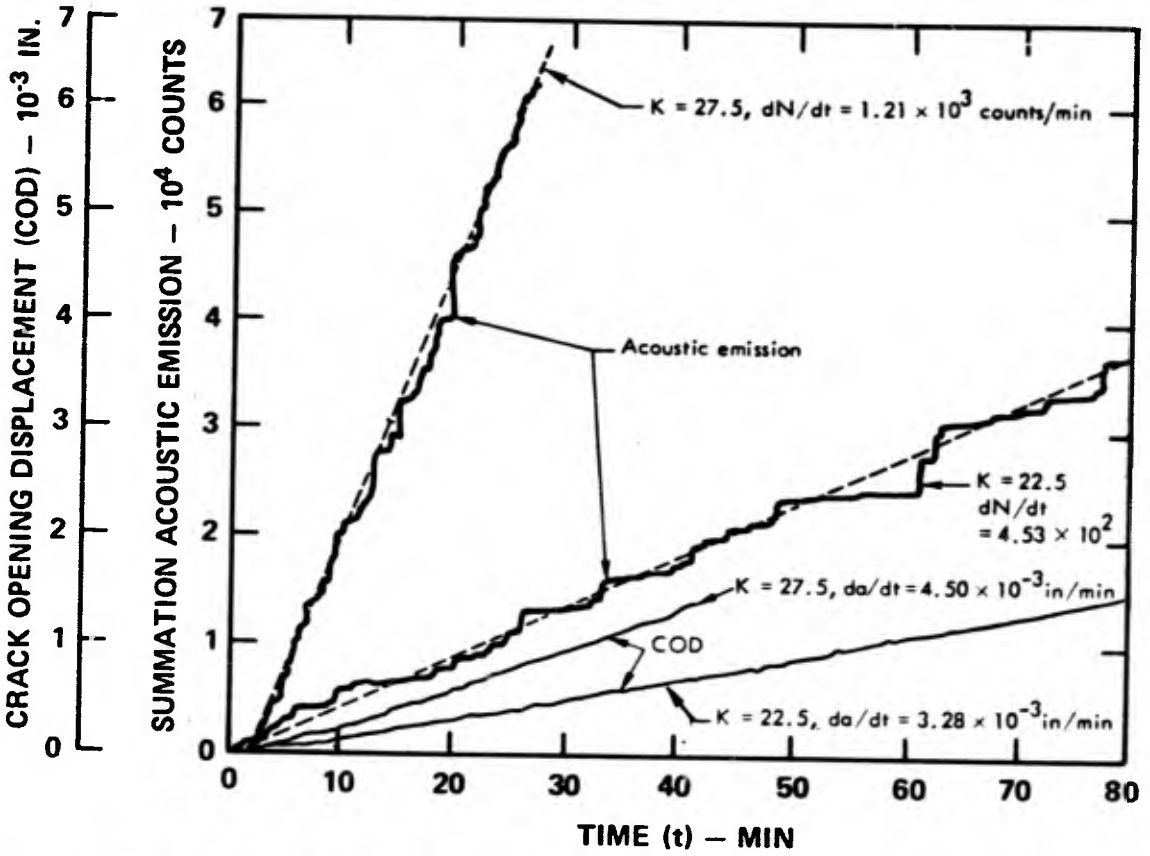

Figure 14. Acoustic Emission and Crack Opening Displacement (COD) as a Function of Time for a Linear Compliance Specimen of 4340 Steel Undergoing Crack Growth due to Hydrogen Embrittlement. Data were Obtained for Two Values of Dead Weight Load, thus Giving Two Values of Stress Intensity K.[14]

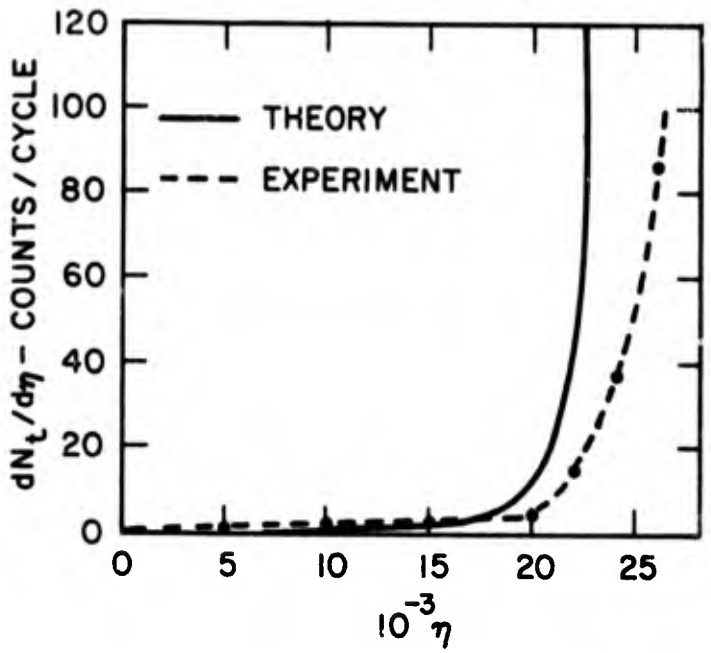

Figure 15. Experimental and Theoretical Results of $dN_t/d\eta$ versus the Number of Fatigue Cycles η [26]

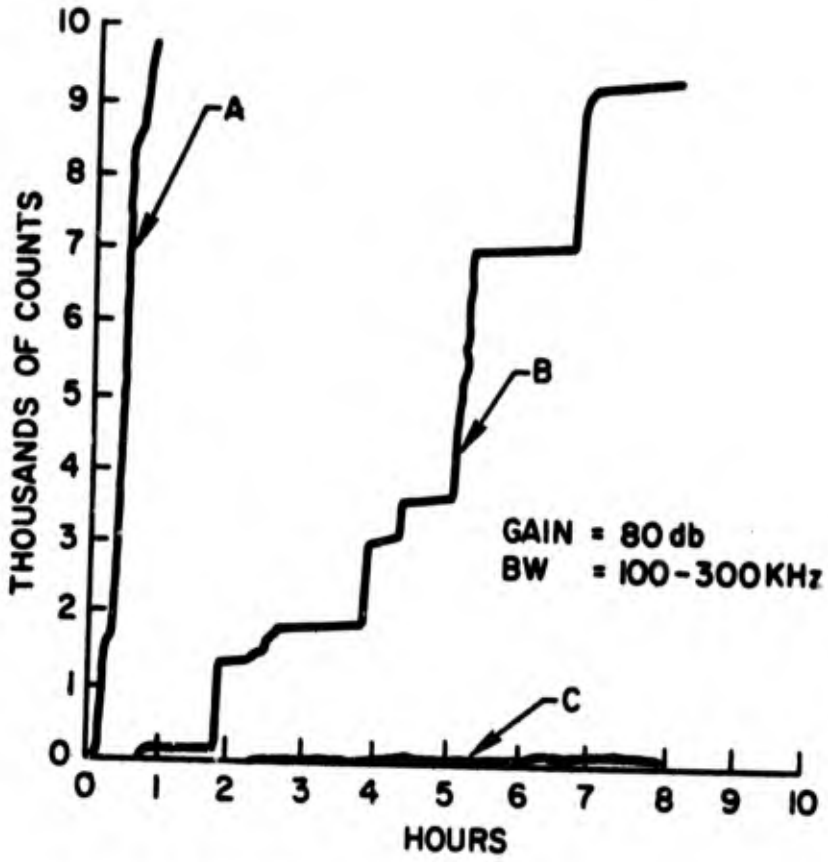

Figure 16. Summation of Acoustic Emission as Function of Time for Three Different Heat Treated Specimens of an Aluminum Alloy under Load in 3 percent Salt Solution(30)